Journal of Engineering Mathematics **30:** 417–443, 1996.
© 1996 *Kluwer Academic Publishers. Printed in the Netherlands.*

Solidification of aluminium spray-formed billets

An analysis of thin layering effects

I.A. FRIGAARD*
Abteilung für Industriemathematik,
Johannes-Kepler-Universität,
Linz, Austria.

Received 1 December 1993; accepted in revised form 18 July 1995

Abstract. A critical part of the billet spray-forming process is the successive intermittent deposition of thin layers of semi-solid aluminium alloy at different points on the top surface of the billet. Each thin layer is made up of a large number of impacted semi-solid spray droplets. As successive layers of alloy are deposited significant re-melting and re-freezing of underlying layers can occur. If the layers become too dry, high porosity will result; if they are too wet, fluid dynamic surface instabilities are possible. In extreme cases no billet will form. The process is essentially incremental, so that heat fluxes within the deposit very close to the top surface play a major role in determining the final deposit microstructure.
In this paper transient heat transfer and solidification processes in the billet are analysed. First, some general features of billet heat transfer are discussed. The focus then narrows onto a thin layer of the deposit, lying very close to the billet surface. A boundary layer approximation is derived and computational results from this approximation are used to answer a number of questions of high practical value.
Key words: Spray-forming, solidification, thin layering

1. Spray-forming

Spray-forming is a metal manufacturing process which is capable of producing large bulk deposits of various alloys. With careful control, rapidly solidified near-net shape deposits can be produced which have significantly improved microstructural and mechanical properties, (see e.g. [1, 2, 3, 4, 5, 6, 7, 8]).

In the billet spray-forming process a molten metal stream is first atomised by high speed gas jets and is then deposited onto a circular collector plate. The collector plate is positioned some distance from the atomiser, it rotates about a vertical axis and is withdrawn slowly downwards at a controlled speed. Usually, the metal spray is directed in towards the rotational axis and oscillates, so as to distribute the metal in a prescribed way. Provided the oscillatory motion of the spray and the rotation of the billet do not synchronise, a cylindrically shaped *billet* forms after a sufficiently long time, Fig. 1.

Spray-forming avoids many safety and contamination problems associated with production of dense bulk aluminium deposits by a powder metallurgy route. An inert gas is used to atomise the liquid metal and the bulk metal is wholly formed in a sealed chamber. Thus, the inclusion of exceptionally high levels of either reactive alloying elements, (e.g. lithium, [9]), and/or reinforcing particulate, (e.g. silicon, [8]), is possible. Advantages of spray-forming over more conventional casting methods are offset by greater production costs, lower throughputs and

* Present address: Schlumberger Cambridge Research, High Cross, Madingley Road, Cambridge, CB3 0EL, U.K.

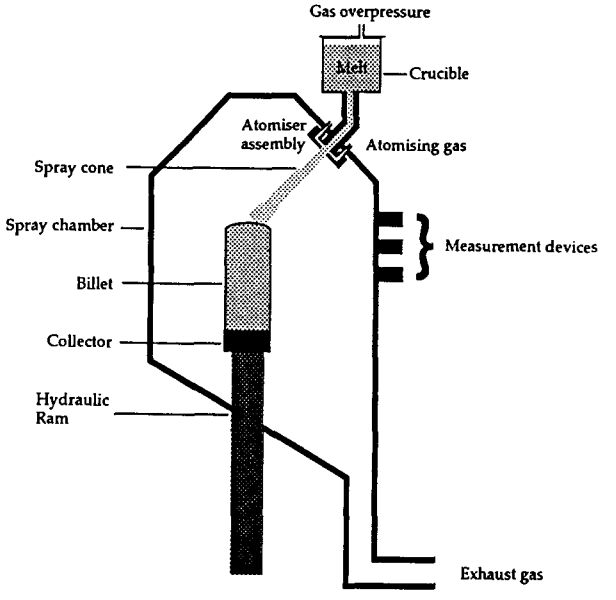

Fig. 1. Schematic of an aluminium billet spray-forming plant

more difficult process control. However, these disadvantages are outweighed by significant mechanical and microstructural improvements, which provide the main motivation for the production method.

Solidification of spray-formed deposits has been investigated widely for deposits which are somehow "thin" and/or one-dimensional, e.g. tubes, strip and discs [10, 11, 12, 13, 14, 15, 16, 17]. This means that intermittent deposition/layering at the deposit surface is able to affect heat flow within the entire deposit. In the case of a billet, the bulk deposit is large relative to the diffusive length-scales of aluminium alloys on the timescale of the intermittent deposition, and should remain largely unaffected by thin layering.

The deposition stage of the process, when the spray impacts the billet surface, is probably the least understood but also most critical stage of the process. Typical spray-formed aluminium alloys release their latent heat of freezing over a wide temperature range, (e.g. 50 – 100°C is not uncommon). If all the spray droplets are fully solid on impact they will not adhere to the billet surface, (which will be colder and drier than the spray). Equally well, a fully liquid deposit is very likely to be spun off the rapidly rotating collector. Therefore, one requires the spray to be partly liquid on deposition. Note however, that additional heat in the spray results in additional heat flowing into the billet, affecting both the surface condition and the spray condition at the point of impact. This suggests that the process will be relatively sensitive to changes in the heat of the depositing spray.

Assuming that one has a reasonably solid "mush" on the billet surface, so that the billet forms satisfactorily, one must still be very careful to avoid porosity development. Porosity in spray-forming is not usually extreme but since high end-product quality is here paramount, porosity can be a major processing concern. As discussed by Lavernia [18], porosity can form due to both the billet/spray being "too dry", (intersticial pores are found), and due to the billet/spray being "too wet", (gas may be trapped in the billet, probably resulting from surface fluid instabilities). The morphology of both types of porosity is distinct and although quantitative understanding of what "too dry" and "too wet" actually mean is largely lacking,

qualitative understanding is quite good. Mathur distinguishes four operational regimes, with deposit formation only occurring in the middle two, [15]. For "dry" deposition, partially solidified droplets impact the surface separated by a time interval which is larger than that required for droplet solidification. The droplets do splat and weld together, but the grains are columnar and do not extend across boundaries inter-splat boundaries. Interstitial microporosity is often observed at inter-splat boundaries. "Wet" deposition occurs when the surface does not fully solidify between impacts, but a high solid fraction present in the surface mush still restricts lateral fluid flow. Inter-splat boundaries are not visible, porosity is minimal and the grains are equiaxed. Singer and Evans have attempted to quantify this distinction, [19].

There are clearly many different degrees of "dry" and "wet" deposition, and although the "wet" regime is in some sense optimal, experience suggests that for many materials the operating window between this regime and the two types of porosity formation, (i.e. "too wet" or "too dry"), is relatively narrow, [20, 21]. As well as influencing porosity levels, the cooling rates close underneath the billet surface will control microsegregation and also will strongly influence the grain size. Perhaps it should also be mentioned that from the commercial point of view "optimal" means producing a material with the mechanical properties which the customer wants; micro-structure is in this sense an invisible intermediate parameter.

For the above reasons, an understanding of sub-surface heat flow is extremely important for the billet spray-forming process. In particular, one would like to understand how one can change the atomiser oscillation and rotation frequencies in order to effectuate desired changes in the heat flow. These frequencies are in a sense free parameters for the process. Common sense dictates only that the scanner and rotation motions do not synchronise and that the frequencies be fast enough that the spray deposition is averaged, (in a naive sense), over the surface. In [22, 23] a model for the averaged growth of axisymmetric billets was developed, and explored further in [24, 25]. In this model the effects of differing atomiser scanner frequencies and rotation rates do not appear at highest order, due to the averaging. Instead, intermittent layering on the surface is described by a "fast-time" perturbation of the averaged growth. In this paper thin layering effects are explored by computing the perturbed transient growth of the billet surface and coupling this with computation of the resulting transient sub-surface heat flow. An important question is how the averaged motions of the billet surface can affect the sub-surface heat flow, and whether this has implications for sensibly choosing a billet shape which is optimal in some sense. Ongoing research work [26] is aimed at the inverse problem of how to reliably design an atomiser scanning function which, when averaged, will produce a steady state billet crown of desired shape.

The article is structured as follows. In the next section some general features of billet solidificiation are discussed. Section 3 derives a boundary layer approximation which controls heat flow close to the billet surface, during and after deposition of thin layers of spray. In section 4 computational results are presented showing how the boundary layer approximation can be used to gain a clear understanding of the sub-surface heat flow. The paper concludes with a discussion. Throughout, a hat (i.e. $\hat{}$) is used to denote a dimensional quantity and bold typeface denotes a vector quantity.

2. Billet solidification

In agreement with other studies of spray-forming, (e.g. [10, 11, 12, 13, 14, 15, 27, 17]), it is assumed that heat flow within the billet is dominated by conduction, The billet volume is

denoted by $\Omega(\hat{t})$ and coordinates fixed to the collector are denoted by $\hat{\mathbf{x}}$. The billet temperature $\hat{T}$ satisfies

$$\frac{\partial \hat{H}}{\partial \hat{t}} = \hat{\nabla}.[\hat{K}\hat{\nabla}\hat{T}], \qquad \hat{\mathbf{x}} \in \Omega(\hat{t}), \tag{1}$$

where $\hat{H}(\hat{T})$ and $\hat{K}(\hat{T})$ are the enthalpy and the thermal conductivity, respectively. For suitable liquid fraction functions, $\hat{H}$ is a strictly monotone function of $\hat{T}$ and may instead be used as the main dependent variable. Equation (1) becomes

$$\frac{\partial \hat{H}}{\partial \hat{t}} = \hat{\nabla}.[\hat{D}(\hat{H})\hat{\nabla}\hat{T}(\hat{H})], \qquad \hat{\mathbf{x}}_0 \in \Omega(\hat{t}), \tag{2}$$

where the diffusivity $\hat{D}(\hat{H})$ is a positive function defined by

$$\hat{D}(\hat{H}) = \hat{K}(\hat{T})\frac{\mathrm{d}\hat{T}}{\mathrm{d}\hat{H}}. \tag{3}$$

The billet surface, $\partial\Omega(\hat{t})$, is described by

$$\partial\Omega(\hat{t}) = \{\hat{\mathbf{x}} \in \mathcal{R}^3 : \hat{F}(\hat{\mathbf{x}}, \hat{t}) = 0\}, \tag{4}$$

where evolution of $\hat{F}$ is governed by the model in [22, 23]. The simplifying assumption is made that the molten spray droplets impinge and coalesce instantaneously[1] onto the infinitesimally thin surface layer. The net flux of heat across $\partial\Omega(\hat{t})$, due to deposition from the spray, at a point $\hat{\boldsymbol{x}}_P \in \partial\Omega(\hat{t})$ which moves normal to the surface at speed $\hat{v}_{\hat{\boldsymbol{x}}_P}$, is equal to

$$\hat{v}_{\hat{\boldsymbol{x}}_P}[\hat{H}_{spray} - \hat{H}(\hat{\boldsymbol{x}}_P, \hat{t})], \tag{5}$$

where $\hat{H}_{spray}$ is the mass averaged enthalpy of the spray, (i.e. averaged over the local droplet distribution in the spray depositing at $\hat{\boldsymbol{x}}_P$). The billet surface is cooled by a combination of radiation and forced convective cooling from the atomising gas.[2] A linear heat transfer law is assumed to account for the net flux of heat out of $\Omega(\hat{t})$ due to combined cooling effects, i.e.

$$\hat{h}_{gas}(\hat{T}(\hat{H}) - \hat{T}_{gas}), \tag{6}$$

where $\hat{h}_{gas}$ and $\hat{T}_{gas}$ are heat transfer coefficient and gas temperature, respectively. Combining (5) and (6) gives

$$-\hat{D}(\hat{H})\frac{\partial \hat{H}}{\partial n} \equiv -\hat{K}(\hat{T})\frac{\partial \hat{T}}{\partial n} = \hat{h}_{gas}[\hat{T}(\hat{H}) - \hat{T}_{gas}] + \hat{v}_{\hat{\boldsymbol{x}}_P}[\hat{H}_{spray} - \hat{H}(\hat{\boldsymbol{x}}_P, \hat{t})]; \tag{7}$$

the operator $\frac{\partial}{\partial n}$ denoting the partial derivative in the direction of the outward normal $\partial\Omega(\hat{t})$.

It should be remarked that the reality of depostion is extremely complicated, with each surface point experiencing irregularly interspersed time intervals during which droplet deposition and forced convective cooling are taking place. Thus, the validity of using (7), (as in [10, 11, 13, 14, 15, 27, 17]), although intuitively correct, is not proven.

The line $z_0 = 0$ represents the boundary between billet and collector, where, due to shrinkage, there will be imperfect thermal contact, i.e.

$$\hat{D}(\hat{H})\frac{\partial \hat{H}}{\partial z_0} \equiv -\hat{K}(\hat{T})\frac{\partial \hat{T}}{\partial n} = \hat{h}_{collector}(\hat{T}(\hat{H}) - \hat{T}_{collector}), \tag{8}$$

with obvious notation.

2.1. NON-DIMENSIONALISATION

The model equations are made dimensionless before any further analysis is carried out. The billet radius $\hat{R}$ is chosen as a length-scale and time is scaled with the period of rotation of the billet, $2\pi/\hat{\omega}$; usually $2\pi/\hat{\omega} \sim \hat{t}_s$, where $\hat{t}_s$ is the period of the atomiser scanning motion. The solidus and liquidus temperatures, freezing range, liquid and solid phase thermal conductivity, density and specific heat capacity, are denoted by $\hat{T}_s$, $\hat{T}_l$, $\Delta\hat{T}$, $\hat{K}_l$, $\hat{K}_s$, $\hat{\rho}$ and $\hat{c}$, respectively; the latter three quantities are measured at close to the solidus temperature. Dimensionless enthalpy, diffusivity and temperature functions are defined by

$$H = \frac{\hat{H} - \hat{H}_s}{\hat{\rho}\hat{c}\Delta\hat{T}}, \qquad D(H) = \frac{\hat{\rho}\hat{c}}{\hat{K}_s}\hat{D}(\hat{H}), \qquad T(H) = \frac{\hat{T}(\hat{H}) - \hat{T}_s}{\Delta\hat{T}}, \tag{9}$$

where $\hat{H}_s$ is the solidus enthalpy. One sees that the alloy is fully solid for $T \leq 0$ or $H \leq 0$, and is fully liquid for $T \geq 1$ or $H \geq 1 + \frac{\hat{L}}{\hat{c}\Delta\hat{T}}$, where $\hat{L}$ is the latent heat of freezing. For many aluminium alloys which are typically sprayed the non-dimensional quantity

$$\frac{\hat{L}}{\hat{c}\Delta\hat{T}} \approx 3.$$

This represents the ratio of latent heat to specific heat which is released during freezing. In this paper intra-alloy variations are not explored and attention is instead confined to a somewhat typical alloy,[3] with non-dimensional functions $T(H)$ and $D(H)$ as illustrated in Fig. 2. Other relevant thermophysical data for this alloy is given in Table 1.

Equations (2), (7) and (8), describing heat flow within the billet on the rotation timescale, become

$$\frac{\partial H}{\partial t} = \frac{\epsilon}{Pe}\nabla.[D(H)\nabla H], \qquad \boldsymbol{x} \in \Omega(t), \tag{10}$$

$$-D(H)\frac{\partial H}{\partial n} = B_{gas}(T(H) - T_{gas}) + \frac{Pe}{\epsilon}v_{\boldsymbol{x}_P}(H - H_{spray}), \quad \boldsymbol{x} \in \partial\Omega(t) : z > 0, \tag{11}$$

$$D(H)\frac{\partial H}{\partial z} = B_{collector}(T(H) - T_{collector}), \qquad \boldsymbol{x} \in \partial\Omega(t) : z = 0. \tag{12}$$

Billet growth is governed by the model in [22, 23]; $v_{\boldsymbol{x}_P}$ is given by

$$v_{\boldsymbol{x}_P} = -\frac{\partial F}{\partial t}|\nabla F|^{-1},$$

where the billet surface $F(\boldsymbol{x}, t) = 0$, satisfies

$$\frac{1}{\epsilon}\frac{\partial F}{\partial t}(\boldsymbol{x}, t) = \gamma(\dot{m}g\boldsymbol{k}', F)\dot{m}(t)g(r'[\boldsymbol{x}, t])\boldsymbol{k}'(t).\nabla F(\boldsymbol{x}, t), \qquad \boldsymbol{x} \in \partial\Omega(t). \tag{13}$$

In (13) γ is a simplified shadowing coefficient and $\dot{m}(t)$ is the mass flow rate through the atomiser. The coordinate r' measures distance perpendicular to the spray cone axis, and $\boldsymbol{k}'$

Table 1. Alloy thermophysical parameters

$\hat{T}_s$	541°C	$\hat{K}_s$	151W/m/°C
$\hat{T}_l$	631.8°C	$\hat{K}_l$	80W/m/°C
$\hat{\rho}$	2400kg/m^3	$\hat{c}$	1180J/kg/°C
$\hat{L}$	317400J/kg		

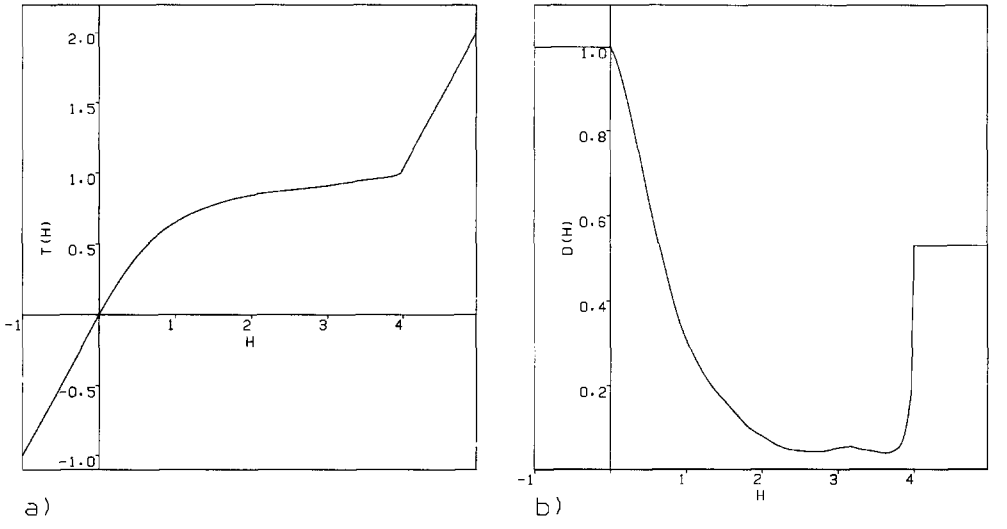

Fig. 2. Temperature and diffusivity functions for a typical aluminium alloy; a) $T(H)$, b) $D(H)$.

is the unit vector in the direction of the spray cone axis at time t. The function $g(r')$ defines the mass flux distribution within the spray cone, which is itself defined by $r' \in [0, r_s)$. All functions are non-dimensional. These terms are explained fully in [22, 23].

2.1.1. *Dimensionless groups*

The two dimensionless groups that appear above in (10) are

$$\epsilon \equiv \frac{2\pi \hat{U}_0}{\hat{\omega}_0 \hat{R}} \ll 1, \tag{14}$$

which is the ratio of the rotation and withdrawal timescales, and

$$Pe \equiv \frac{\hat{\rho}\hat{c}\hat{U}_0\hat{R}}{\hat{K}_s} = (\frac{\hat{R}}{\hat{U}_0})^{-1}(\frac{\hat{\rho}\hat{c}\hat{R}^2}{\hat{K}_s}), \tag{15}$$

which is a Peclet number. It is the smallness of ϵ which prompted the use of an averaging method in [22, 23, 24, 25]. The size of ϵ essentially corresponds to the thickness of the thin layers deposited, relative to $\hat{R}$.

After rescaling time with ϵ in (10), it is seen that the Peclet number compares the relative importance of conduction and convection within the bulk billet. Convective effects in this

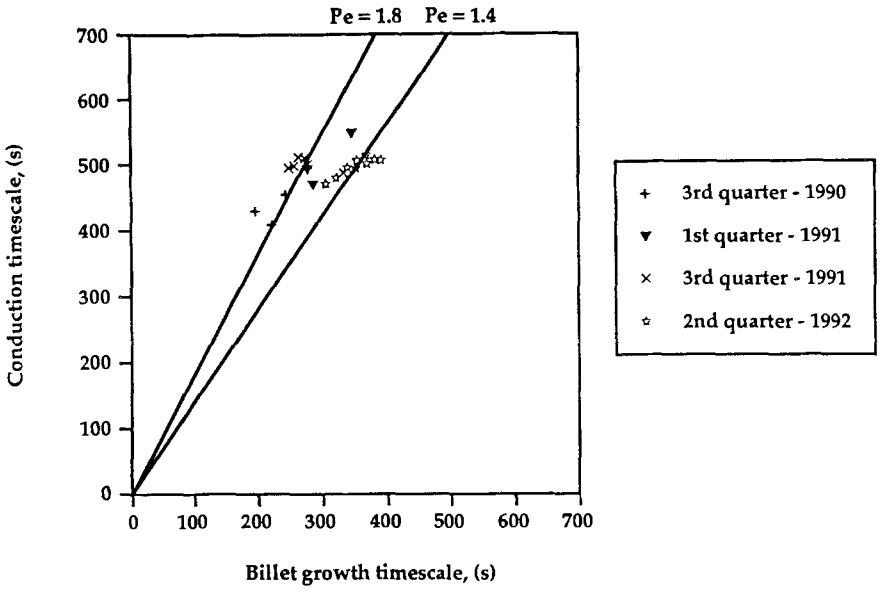

Fig. 3. Comparison of billet growth timescale and conduction timescale for a number of successful spraying runs on Alcan International's production plant in Banbury, UK.

context are due to billet growth, which occurs at a rate $\approx \hat{U}_0$. An alternative interpretation of the Peclet number is as the ratio of the timescales for conduction/solidification and for billet growth. A large Peclet number would imply that the solidification timescale is longer than the growth timescale resulting in a billet with a high liquid fraction. Conversely, a small Peclet number would imply that heat flowing in through the billet crown is rapidly dissipated in the bulk of the billet. The billet may in this case be very dry. Not surprisingly, for typical production parameters $Pe = O_S(1)$. In Fig. 3 are plotted values of $R/\hat{U}_0$ against $\rho c R^2/K_s$, for a number of successful spraying production runs[4] of the aluminium alloy in Fig. 2 and Table 1.

In the boundary condition equations (11) and (12), B_{gas} and $B_{collector}$ are Biot numbers, defined by

$$B_{gas} = \frac{\hat{h}_{gas} R}{K_s}, \tag{16}$$

$$B_{collector} = \frac{\hat{h}_{collector} R}{K_s}. \tag{17}$$

For typical alloys, process conditions and billet radii these can be estimated to have sizes

$$0.3 < B_{gas} < 1.0, \text{ and } B_{collector} \approx 2.0, \tag{18}$$

with the higher values of B_{gas} being experienced on the top surface of the billet, directly under the spray, where $\hat{h}_{gas}$ probably attains a value $\hat{h}_{gas} \approx 1000\text{W/m}^2/^\circ\text{C}$.

3. Boundary layer approximation

There are severe practical limitations to the usefulness of equations (10)-(12) as a model. Analytic solution is clearly not possible, and numerical solution is quite infeasible. The

production run timescale is $O(\epsilon^{-1})$, but the rapid changes occurring in (11) mean that a small timestep must be used in any numerical algorithm. Additionally, whereas in the bulk of the billet one expects only $O(\epsilon)$ enthalpy changes to occur, it is clear from (11) that $O_S(1)$ changes do occur close to the deposition surface at least. Equations (10) and (11) suggest that the process close to the surface is governed by the "fast" rotation timescale. This motivates the following boundary layer approximation.

Consider a point $\boldsymbol{x}_P(t) = (x_P(t), y_P(t), z_P(t))$, lying on the surface of the billet at time t and moving with instantaneous velocity

$$\frac{\mathrm{d}\boldsymbol{x}_P}{\mathrm{d}t}(t) = v_{\boldsymbol{x}_P}(t)\boldsymbol{n}_P(t), \tag{19}$$

where $\boldsymbol{n}_P(t)$ is the unit outward normal vector to the billet surface at $\boldsymbol{x}_P$.

The billet surface position is assumed to have an axisymmetric $O(\epsilon)$ asymptotic approximation, uniformly valid on the timescale ϵ^{-1}, given by the averaged equations of the model developed in [22, 23], i.e.

$$F(\boldsymbol{x}_0, \eta, t) \sim F_0(r, z, \eta) + O(\epsilon), \tag{20}$$

where (r, z) are cylindrical polar billet coordinates and η denotes the "slow-time" variable, $\eta = \epsilon t$. Orthogonal unit vectors $\tilde{\boldsymbol{i}}(t)$, $\tilde{\boldsymbol{j}}(t)$ and $\tilde{\boldsymbol{k}}(t)$ are chosen, fixed at $\boldsymbol{x}_P$, such that

$$\tilde{\boldsymbol{k}}(t) \equiv -\frac{\nabla F_0(\boldsymbol{x}_P, \eta)}{\|\nabla F_0(\boldsymbol{x}_P, \eta)\|} = -\boldsymbol{n}_P(t) + O(\epsilon), \tag{21}$$

with $\tilde{\boldsymbol{i}}(t)$ and $\tilde{\boldsymbol{j}}(t)$ then fixed arbitrarily to form a right handed system. Position with respect to the surface coordinate system is denoted $\tilde{\boldsymbol{x}}$, where

$$\tilde{\boldsymbol{x}} = (\tilde{\boldsymbol{i}}.[\boldsymbol{x}_0 - \boldsymbol{x}_P], \tilde{\boldsymbol{j}}.[\boldsymbol{x}_0 - \boldsymbol{x}_P], \tilde{\boldsymbol{k}}.[\boldsymbol{x}_0 - \boldsymbol{x}_P]). \tag{22}$$

On the rotation timescale it is assumed that tangential thermal gradients[5] are $O(1)$ and that thermal gradients normal to the surface vary on the diffusive length-scale, $(\epsilon/Pe)^{1/2}$. Transient heat flow is considered within an $O((\epsilon/Pe)^{1/2})$ neighbourhood of $\boldsymbol{x}_P$. Distance $\tilde{z}$, in the direction of $\tilde{\boldsymbol{k}}$ is rescaled with this length-scale, thus introducing a boundary layer coordinate ζ, defined by

$$\tilde{z} = \zeta(\frac{\epsilon}{Pe})^{1/2}. \tag{23}$$

Retaining only terms of $O(\epsilon^{1/2})$ and larger, after a little algebra, equations (10) and (11) become

$$\frac{\partial H}{\partial t} + (\frac{Pe}{\epsilon})^{1/2} v_{\boldsymbol{x}_P} \frac{\partial H}{\partial \zeta} = \frac{\partial}{\partial \zeta}[D(H)\frac{\partial H}{\partial \zeta}], \qquad \zeta > 0, \tag{24}$$

and

$$D(H)\frac{\partial H}{\partial \zeta} = (\frac{\epsilon}{Pe})^{1/2} B_{gas}(T(H) - T_{gas}) + (\frac{Pe}{\epsilon})^{1/2} v_{\boldsymbol{x}_P}(H - H_{spray}), \qquad \zeta = 0. \tag{25}$$

An $O(\epsilon)$ approximation to the surface velocity is gained from substituting $F_0(\boldsymbol{x}_0, \eta)$ in the right hand side of (13), i.e.

$$\frac{1}{\epsilon}\frac{\partial F}{\partial t}(\boldsymbol{x}_0, t) \sim \gamma(\dot{m}g\boldsymbol{k}', F_0)\dot{m}(\eta)g(r'[\boldsymbol{x}_0, t])\boldsymbol{k}'(t).\nabla F_0(\boldsymbol{x}_0, \eta) + O(\epsilon). \tag{26}$$

This may be used in (24) and (25) to give an approximate expression for $v_{\boldsymbol{x}_P}$. Defining $v(t)$ and β by

$$v(t) \equiv -\frac{(\epsilon Pe)^{1/2}\gamma(\dot{m}g\boldsymbol{k}', F_0)\dot{m}(\eta)g(r')\boldsymbol{k}'(t).\boldsymbol{\nabla}F_0}{|\boldsymbol{\nabla}F_0|} = (\frac{Pe}{\epsilon})^{1/2}v_{\boldsymbol{x}_P} + O(\epsilon^{3/2}), \tag{27}$$

$$\beta \equiv (\frac{\epsilon}{Pe})^{1/2}B_{gas}, \tag{28}$$

the boundary layer approximation becomes

$$\frac{\partial H}{\partial t} = -v(t)\frac{\partial H}{\partial \zeta} + \frac{\partial}{\partial \zeta}[D(H)\frac{\partial H}{\partial \zeta}], \qquad \zeta > 0, \tag{29}$$

$$D(H)\frac{\partial H}{\partial \zeta} = \beta(T(H) - T_{gas}) + v(t)(H - H_{spray}), \qquad \zeta = 0, \tag{30}$$

$$\frac{\partial H}{\partial \zeta} \to 0, \qquad \zeta \to \infty, \tag{31}$$

where the far-field condition (31) results since, for $\zeta \sim (Pe/\epsilon)^{1/2}$, one expects

$$\frac{\partial H}{\partial \tilde{z}} = O(1). \tag{32}$$

3.1. Comments on the boundary layer approximation

Terms in equation (29) of up to 1st order (in $\epsilon^{1/2}$) have been retained, since the 0th-order approximation is not very interesting. Due to the scaling all dependent thermodynamic variables should be $O(1)$, as should the parameters T_{gas} and H_{spray}; both the boundary layer Biot number, β, and the surface velocity, $v(t)$, are $O(\epsilon^{1/2})$ as $\epsilon \to 0$. In a more complete model β, T_{gas} and H_{spray} could all be considered to vary with both t and $\boldsymbol{x}_P$, but here these parameters will be taken as constant. This is motivated by simplicity and the desire to independently investigate the effects of changing $v(t)$. One might also expect that the variations in β, T_{gas} and H_{spray} will not be as extreme as that in $v(t)$, (i.e. there will always be a certain amount of heat loss to the gas and the variation in H_{spray} across the spray cone is relatively small, [11, 17]).

The scanning and rotation movements interact in depositing metal spray at irregular intervals at point $\boldsymbol{x}_P$. When $\boldsymbol{x}_P$ is not under the spray cone then

$$v(t) = 0,$$

and when $\boldsymbol{x}_P$ is under the spray cone then

$$v(t) \sim (\epsilon Pe)^{1/2}\dot{m}(\eta)g(r').$$

Thus, $v(t)$ has the form of an intermittent pulse. Typically, $\dot{m}(\eta) \approx 1$ and $g(r')$ decreases monotonically to zero in $r' \in (0, r_s)$, with the conservation condition

$$\int_0^{r_s} r'g(r')\mathrm{d}r' = \frac{1}{2}, \tag{33}$$

also being satisfied. Therefore, $g(r') \sim r_s^{-2}$ in $[0, r_s)$, but $g(r')$ is clearly concentrated about $r' = 0$. Since, $r_s \in [1/3, 2/3]$ for usual atomising conditions and other process parameters, it is clear that quite large surface velocities $v(t)$ can be experienced when deposition comes from close to the middle of the spray cone. Thus, although $v(t) \to 0$ uniformly in the limit $\epsilon \to 0$, for the finite values of ϵ which are typical of the real process, ($\epsilon \sim 10^{-3}$), values $v(t) = O_S(1)$ are common. This is a further motivation for considering the 1st order terms in (29). On a much longer timescale the averaging methods used in [22, 23] indicate that time averaged values of $v(t)$, say $\overline{v}$, are $O((\epsilon Pe)^{1/2})$, which then balance approximately with the $O((\epsilon/Pe)^{1/2})$ convective cooling term in (30).

3.1.1. *Validity and limitations*

The boundary layer approximation takes a point, $\boldsymbol{x}_P$, initially at a fixed radial distance from the billet axis of rotation and looks at the heat flow in the direction normal to the surface at that point. As with all such asymptotic approximations, it is expected to be valid in the spatial direction, only for

$$\zeta \ll (\frac{Pe}{\epsilon})^{1/2}. \tag{34}$$

However, there is now also a further restriction on the validity of the approximation in the temporal direction. One reason for this is that the ζ-axis is fixed to $\boldsymbol{x}_P$, and will therefore change its orientation as the surface changes shape. Billet shape changes that are significant in the boundary layer will occur on a timescale $t \sim (\epsilon Pe)^{-1/2}$ Thus, if one wishes to investigate heat flow at fixed *material* points along the ζ-axis, it is required that the total time period, Dt, throughout which the boundary layer equations are integrated satisfies

$$\mathrm{D}t \ll \frac{1}{(\epsilon Pe)^{1/2}}. \tag{35}$$

This restriction is also necessitated by the form chosen for $v(t)$. The function $v(t)$ is found straightforwardly by considering the deposition which would occur over the rotation timescale upon the time averaged billet surface. This is effectively a regular perturbation method, used to get an $O(\epsilon)$ approximation to the growth on the fast timescale and one can only prove this accuracy over an $O(1)$ timescale. Although, one could derive an approximation to the instantaneous surface velocity which remains valid over a longer timescale it would be of little real value, since the aim here is to look at heat flow at fixed material points under the surface.

A last remark is that one should not expect the boundary layer approximation to be valid immediately, during the initial stages of billet growth. In this time period, the collector represents a very effective heat sink, particularly when the billet and boundary layer thickness are comparable.

3.1.2. *Far-field behaviour and boundedness of* $H(\zeta, t)$

The far-field boundary condition, (31), implies that a constant value for H is approached as $\zeta \to \infty$, say $H \to H_\infty$. Suppose that $H \to H_\infty$ sufficiently fast for the improper integral

$$\boldsymbol{H}(t) \equiv \int_0^\infty [H(\zeta, t) - H_\infty] \, \mathrm{d}\zeta, \tag{36}$$

to exist and be differentiable. The functional $\boldsymbol{H}$ is representative of the total heat in the boundary layer. The derivative of $\boldsymbol{H}(t)$ is

$$\frac{\mathrm{d}}{\mathrm{d}t}\boldsymbol{H}(t) = -\beta(T(H(0,t)) - T_{gas}) - v(t)(H_\infty - H_{spray}), \tag{37}$$

from which it is seen that changes in $\boldsymbol{H}(t)$ result from heat losses to the surrounding gas and from convection of heat right through the boundary layer, at speed $v(t)$. The boundary layer represents a region of the billet within which transient heat transfer mechanisms are in operation during deposition and should not "on average" gain or lose heat. To do so would imply a heat source or sink in the boundary layer, which is unrealistic since there are none in the billet as a whole and since the boundary layer heat flow is one dimensional. Hence, (37) averaged over time should equal zero. If the averaged billet shape F_0 is axisymmetric, one might reasonably expect the (averaged) heat fluxes within the billet to be axisymmetric and the average of (37) is then easily computed. Setting this average equal to zero should give the far-field enthalpy H_∞ in terms of the average of $v(t)$ and $T(H(0,t))$; i.e.

$$\beta(\overline{T(H(0,t))} - T_{gas}) + \overline{v}(H_\infty - H_{spray}) = 0. \tag{38}$$

Consider now the time averaged boundary layer equations

$$\frac{\partial H_a}{\partial t} = -\overline{v}\frac{\partial H_a}{\partial \zeta} + \frac{\partial}{\partial \zeta}[D(H_a)\frac{\partial H_a}{\partial \zeta}], \qquad \zeta > 0, \tag{39}$$

$$D(H_a)\frac{\partial H_a}{\partial \zeta} = \beta(T(H_a) - T_{gas}) + \overline{v}(H_a - H_{spray}), \qquad \zeta = 0, \tag{40}$$

$$\frac{\partial H_a}{\partial \zeta} \to 0. \qquad \zeta \to \infty. \tag{41}$$

These equations have a constant steady state solution $H_a(\zeta, t) = \overline{H}$, to which solutions from arbitrary initial conditions converge to as $t \to \infty$, in the norm

$$\boldsymbol{E}(t) \equiv \int_0^\infty [H_a(\zeta, t) - \overline{H}]^2 \, \mathrm{d}\zeta. \tag{42}$$

The constant $\overline{H}$ is the unique solution of

$$\beta(T(\overline{H}) - T_{gas}) + \overline{v}(\overline{H} - H_{spray}) = 0. \tag{43}$$

Comparing (43) with (38) it is seen that

$$\overline{T(H(0,t))} > T(\overline{H}) \;\Rightarrow\; H_\infty < \overline{H},$$

$$\overline{T(H(0,t))} < T(\overline{H}) \;\Rightarrow\; H_\infty > \overline{H}.$$

The above two possibilities both imply a net flow of heat through the boundary layer, respectively into and out of the billet, contradicting the far field boundary condition (31). Hence, it follows that

$$\overline{H} = H_\infty \text{ and } T(\overline{H}) = T(H(0,t)), \tag{44}$$

i.e. the far field boundary layer enthalpy is determined by averaging the boundary condition at $\zeta = 0$.

To examine the departure of the transient boundary layer solution from the far-field enthalpy $\overline{H}$, the norm (42), (with $H_a(\zeta,t)$ replaced by $H(\zeta,t)$), is differentiated, giving

$$\frac{\mathrm{d}}{\mathrm{d}t}\boldsymbol{E}(t) = -2\int_0^\infty D(H)[\frac{\partial H}{\partial \zeta}]^2\mathrm{d}\zeta - [v(t)+2\beta\frac{\mathrm{d}T}{\mathrm{d}H}(H^*)][H(0,t)-\overline{H}]^2$$
$$+ 2[H_{spray}-\overline{H}][v(t)-\overline{v}][H(0,t)-\overline{H}], \tag{45}$$

where $H^*(t)$ is between $H(0,t)$ and $\overline{H}$. The first two terms in (45) are negative always. The third term will be predominantly positive, since periods of time when $v(t) > \overline{v}$ are likely to result in $H(0,t) > \overline{H}$ and $v(t) < \overline{v}$ is likely to result in $H(0,t) < \overline{H}$. Thus, fluctuations from $\overline{H}$ may occur. However, since $|v(t)-\overline{v}|$ is bounded and the second term in (45) is quadratic in $[H(0,t)-\overline{H}]$ it can be seen that fluctuations from $\overline{H}$ will be bounded with respect to the norm $\boldsymbol{E}(t)$.

3.2. NUMERICAL SOLUTION

The boundary layer solution takes the form of a bounded oscillation about the value $\overline{H}$. Due to the nonlinearity of (29) a numerical solution will be necessary. Because of the axisymmetric nature of the billet growth, one is interested mostly in determining the characteristic thermal behaviour of points close to the billet surface at different radial distances from the billet axis of rotation.

3.2.1. *Presolution algorithm*

Suppose one would like to solve the boundary layer equations at $\boldsymbol{x}_P(t)$ for an short time interval $\Delta t = t_2 - t_1 = O_S(1)$, where $t_1 = O_S(\epsilon^{-1})$ is some time during the process run. Two pieces of data are missing. First, at t_1 initial conditions must be specified and second, if $\boldsymbol{x}_P(t_1)$ has radial and vertical coordinates (r,z), the azimuthal coordinate ϕ_0 must also be specified.

It is clearly impossible to impose the "correct" initial conditions at t_1, since these are completely unknown. However, the boundary layer approximation is in a sense *forced* by the deposition boundary condition. This suggests that a sensible procedure would be to assign the far-field enthalpy value $\overline{H}$, as initial condition at an earlier time $t_0 < t_1$, and compute the numerical solution over the interval $[t_0,t_2]$. Because (29) is inherently diffusive the initial error will decay rapidly with time, (*c.f.* countless linear heat equation analogies), and the solution observed at t_1 should provide a realsitic estimate for the "correct" initial condition. The far-field enthalpy $\overline{H}$, $(= H_\infty)$, is found by solving the nonlinear equation (43).

In order to specify ϕ_0, first note that $v(t)$ will vary with choice of ϕ_0, although its time-average $\overline{v}$ depends only on (r,z). Because one wants the solution to be representative of the heat fluxes at (r,z) one should choose ϕ_0 such that the average of $v(t)$ taken over the computational interval is equal to $\overline{v}$. Since initial conditions are to be assigned at t_0 the computational interval is $[t_0,t_2]$. Therefore, one finds ϕ_0 through numerical solution of

$$[t_2-t_0]\overline{v} = \int_{t_0}^{t_2} v(r,z,\phi_0,t)\,\mathrm{d}t. \tag{46}$$

When finding the initial condition through solution of (43) and in solving (46) the value of $\overline{v}$ is taken at $t = t_1$ although, since $\overline{v} \sim \epsilon^{1/2}$ and over any $O_S(1)$ time interval $\overline{v}$ changes only by an amount of $O(\epsilon^{3/2})$, any $t \in [t_0,t_2]$ could be used.

For a given rotation and scanner motion, one could of course also consider azimuthal variations in thermal behaviour, (i.e. dispense with (46) and select ϕ_0), but the reason for doing this is to investigate the asymmetry of the layering over a short time period, which is a secondary question.

3.2.2. *Solution algorithm*

Selection of ϕ_0 and setting initial conditions at t_0 are the presolution algorithm, which must be carried out before (29) can be integrated. The presolution algorithm also clearly requires computation of the averaged billet growth, by the methods described in [22, 25]. The efficiency with which ϕ_0 is found may be easily monitored;

$$\frac{1}{(\epsilon Pe)^{1/2}} \left| [t_2 - t_0] \times \overline{v} - \int_{t_0}^{t_2} v(r, z, \phi_0, t)\, \mathrm{d}t \right| \sim 10^{-4}, \tag{47}$$

being a typical accuracy for the results of this paper.

For integration of (29) a two-stage, two-level finite difference method is used. This method is a simple adaptation of the CPC and MPC predictor-corrector schemes described in [31]. The method is consistent and has a local truncation error $O(\Delta t^2) + O(\Delta \zeta^2)$. Convergence of the scheme is not proven here, but the methods used in [31] should straightforwardly demonstrate that convergence in the time direction is at least $O(\Delta t^{3/2})$, and is $O(\Delta \zeta^2)$ spatially. See [22] for a full description of the algorithm. For all the computations presented in this paper a mesh spacing $\Delta \zeta = .02$ has been used. Further mesh refinement produces little effect, and for the far-field boundary conditions imposed there is a negligible departure of the enthalpy from its far-field value, computed from (43). The (variable) time step Δt is chosen so that $\Delta t \sim \Delta \zeta$, but is also shortened during periods when $v(t) > 0$, in order not to miss the spray pulse. The semi-infinite spatial domain, $\zeta \in [0, \infty)$ is replaced by the finite computational domain $\zeta \in [0, 3]$. One important reason for choosing the particular numerical scheme of Meek and Norbury over others is that there is no need to evaluate derivatives of the functions $D(H)$ and $T(H)$. This becomes important when these functions have been approximated from experimental data.

4. Computational results

All following computations use the aluminium alloy in Fig. 2 and Table 1. The Peclet number is fixed at $Pe = 1.8$; $H_{spray} = 1.981$ is selected to correspond to the spray having on average 50% liquid fraction on deposition; $T_{gas} = -3.755$ corresponds to a gas temperature, (close to the billet surface), of 200°C. These parameters are believed to be representative of those found on production plants.

4.1. Radial heat flow variations

Here, typical radial heat flow variations are explored. It is assumed that the the underlying billet growth is controlled by constant mass flow and withdrawal rates, $\dot{m} = 1$ and $u = 1$. The billet grows towards a steady state of radius $r_b = 1$, see [22, 23, 24]. The boundary layer heat flow is computed at four radial distances from the billet axis of rotation, $r = 0$, 0.25, 0.5 and 0.75. A time interval corresponding to three rotations of the billet is chosen.

In Fig. 4a the scanner angle function $\alpha(t)$ is shown. The spray cone axis makes an angle $a(t) = \alpha_1 + \alpha_2 \alpha(t)$ with the vertical $-z$ axis, where here $\alpha_1 = 35°$ and $\alpha_2 = 6°$. After

averaging, assuming a spray cone radius $r_s = 1/3$, the shape of the steady state to which the billet will grow is shown in Fig. 4b, together with the spray boundaries. It can be seen that, apart from a slight "kink" at mid-radius the billet crown is nearly horizontal. For the heat flow computations to follow a value $\epsilon = 10^{-3}$ is assumed and $\beta = 0.0187 \sim (\epsilon/Pe)^{1/2}$, which corresponds to $\hat{h}_{gas} \approx 800\text{W/m}^2/^\circ\text{C}$ for a 0.15m radius billet. In Figs. 4c and 4d are shown the locus of the intercept of the spray cone axis ($r' = 0$) with the steady state surface shown in Fig. 4b, for a time interval $\Delta t = 3$; the scanner period has been chosen as $t_s = 5/17$ and $t_s = 7/60$, respectively.

Fig. 5 shows plots of the surface normal velocity $v(t)$ and the billet growth normal to the surface, say $\zeta_g(t)$:

$$\zeta_g(t) = \int^t v(\tau)\, \mathrm{d}\tau. \tag{48}$$

Figs. 5a, c, e & g compare the averaged and instantaneous billet growth in the normal direction. Figs. 5b, d, f & h, show the different functions $v(t)$ computed. At all four radial distances it can be seen that the average of $v(t)$ over the full interval corresponds to the averaged growth. Also one can see that the velocity pulses $v(t)$ are intermittent and are commonly $O_S(1)$. The velocity pulse at $r = 0$, Fig. 5b, is very regular. From Fig. 4c, one can see that the spray should hit the centre of the billet 3.4 times each rotation, (imagine a spray cone of radius $\approx 1/3$ following this locus). The velocity pulses at $r = 0.25$, 0.5 and 0.75, (Figs. 5d, f & h), are much more irregular, but may also be interpretted with reference to the "flower pattern" of Fig. 4c.

Fig. 6 shows heat fluxes at each of the four radial positions. In each of Figs. 6a, b, c & d the top part of the figure shows a plot of the computed billet surface temperature $T(0,t)$, over the time interval $\Delta t = 3$, superimposed upon the computed far-field temperature, (recall $T = 0$ is the solidus temperature, $T = 1$ is the liquidus temperature). In the lower pictures have been plotted the effect of the heat flow on the sub-surface billet. In the lower pictures, the horizontal axis again denotes time over the interval $\Delta t = 3$. The vertical axis measures distance above the position of the billet surface at $t = t_1$, i.e. the billet growth has been computed from $t = t_1$ and this has been subtracted away from the ζ-coordinate, so that the resulting vertical axis shows the real physical depth $\zeta_g(t) - \zeta$, within the billet. The thick black line shows the billet surface position, growing "upwards" in the normal direction during this time interval. Below the thick black line have been plotted the isotherms of the computed thermal fields. Isotherms are plotted at intervals which correspond to 1% of liquid fraction of the alloy, (when semi-solid), and at intervals corresponding to 5% of the freezing range of the alloy, (when fully solid).

Most noticeable in comparing Figs. 5 and 6 is that the surface temperature transient mimics the surface normal velocity pulse, as is to be expected. However, fluctuations in surface temperature are characterised by sharp rises, due to rapid heating by the metal spray pulse, followed by slower decays caused by gradual domination of gas cooling as the pulse dies away. That there is no overall rise in surface temperature with time, but rather an oscillation about the far field temperature, confirms numerically the analysis of section 3.1.2, leading to the definition of $\overline{H}$.

The far-field temperatures at $r = 0$, 0.25 & 0.75 are almost identical, that at $r = 0.5$ is however lower. The reason for this is because the averaged normal velocity at $r = 0.5$ is also lower, (compare Fig. 5e with Figs. 5a, c & g). This difference results only from the very slight slope of the billet surface at $r = 0.5$, see Fig. 4b. If the billet is growing with a

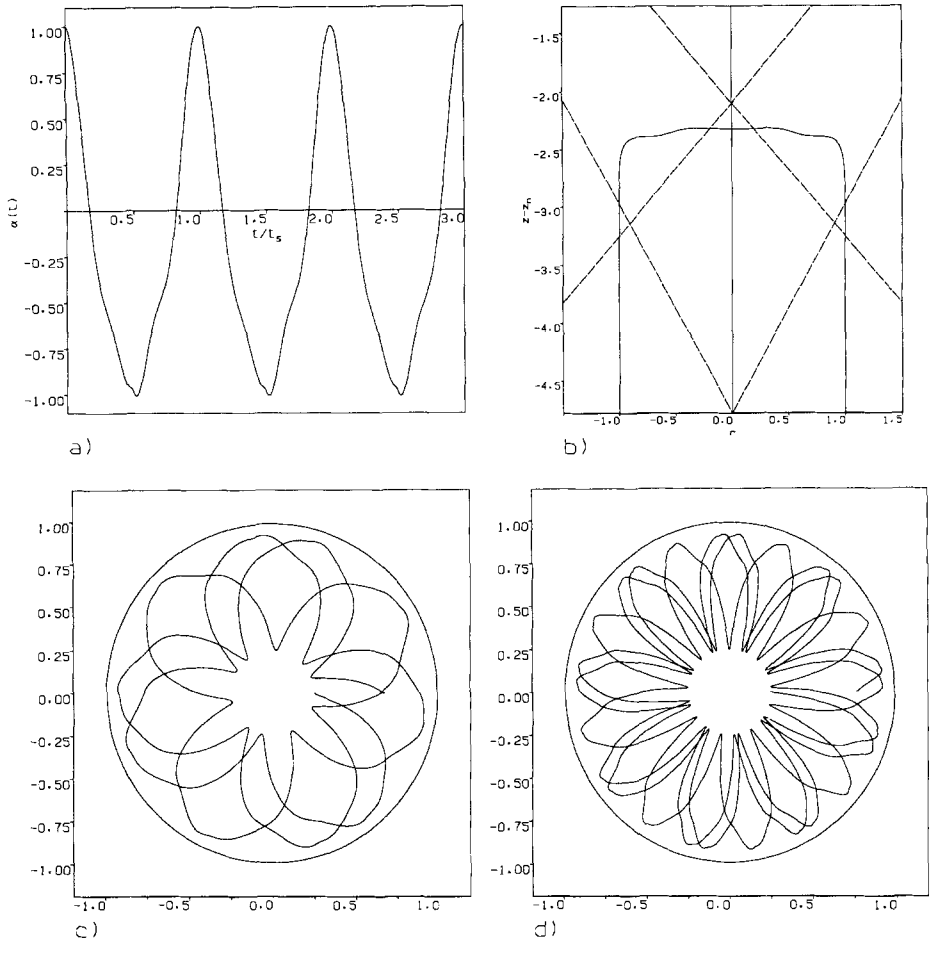

Fig. 4. a) scanner angle function, $\alpha(t)$; b) steady state surface, $\alpha_1 = 35°$ and $\alpha_2 = 6°$, $r_s = 1/3$, $g(r')$ truncated normal distribution, dotted lines are spray boundaries, vertical axis measures distance $z - z_n$ below atomiser nozzle; c) Locus of the intercept of the spray cone axis with the steady state surface shown in b: $t_s = 5/17$; d) Locus of the intercept of the spray cone axis with the steady state surface shown in b: $t_s = 7/60$.

steady state crown shape, then at all points where the surface is horizontal the surface normal velocity is clearly equal to the withdrawal speed. However, at points where the surface is sloped the surface normal velocity is smaller than the withdrawal speed. The change in slope in Fig. 4b appears insignificant, but translated into dimensional terms the difference in far field temperatures is about 4 – 5°C.

At the billet centre, Fig. 6a, the small rapid deposition pulses are seen to result in only a very small regular penetration of the 4% isotherm into the billet. At greater radial distances, Figs. 6b, c & d, the larger surface temperature variations result in much deeper pulse penetration. Also noticeable here are the characteristic triangular isotherms during the periods of cooling.

4.2. CHANGING ROTATION AND SCANNER FREQUENCIES

One would like to know what the effects are of varying the rotation and scanner frequencies. Clearly any variation in either scanner or rotation frequency alone will change the velocity pulse pattern experienced at any particular surface point. The range of different possible

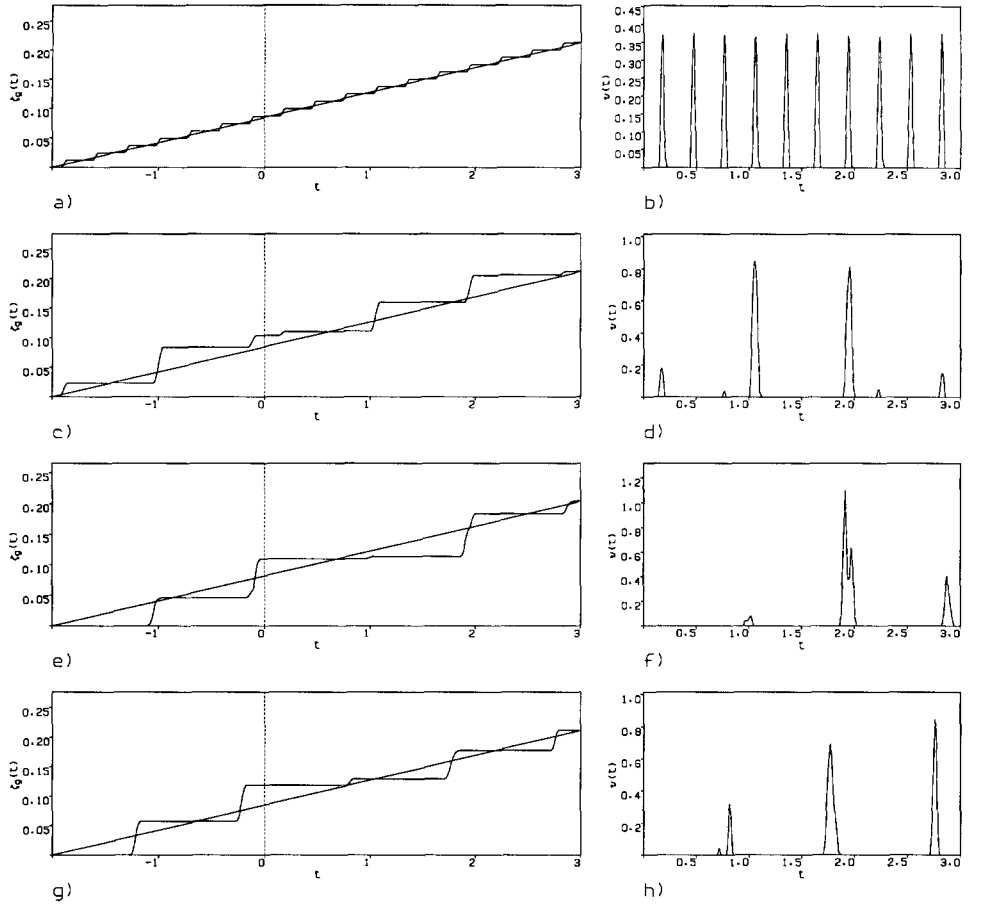

Fig. 5. Comparison of instantaneous and averaged growth: a) $r = 0$, c) $r = 0.25$, e) $r = 0.5$, g) $r = 0.75$; surface normal velocity, $v(t)$: b) $r = 0$, d) $r = 0.25$, f) $r = 0.5$, h) $r = 0.75$. All figures $t_s = 5/17$.

velocity pulse patterns will then be inexhaustable. Here instead, the two parameters are changed together. This has the effect of varying ϵ, whilst leaving other parameters unchanged, i.e. "What happens if we speed up the rotation/scanning?".

Here identical computations to those in section 4.1 have been carried out for the two values $\epsilon = 3 \times 10^{-3}$ and $\epsilon = 3.333 \times 10^{-4}$. To maintain the same physical cooling effect, the boundary layer Biot number for the two values of ϵ is adjusted to $\beta = 0.03244$ and $\beta = 0.01081$, respectively. All other parameters remain unchanged.

Variation of ϵ has two effects on the physical interpretation of results from the boundary layer approximation. Firstly, the physical timescale is proportional to ϵ. Secondly, the physical length-scale is proportional to $\epsilon^{1/2}$. In the following computations the same physical time interval is retained for both values of ϵ, corresponding to one and nine rotation periods for $\epsilon = 3 \times 10^{-3}$ and $\epsilon = 3.333 \times 10^{-4}$, respectively. For the plots of the sub-surface isotherms, the physical length-scale corresponding to $\epsilon = 3 \times 10^{-3}$ will be three times as large as that corresponding to $\epsilon = 3.333 \times 10^{-4}$.

Fig. 7 shows the variation in far field temperature, surface temperature and sub-surface heat flow at radial positions $r = 0$, 0.25, 0.5 and 0.75, for $\epsilon = 3 \times 10^{-3}$, computed over a

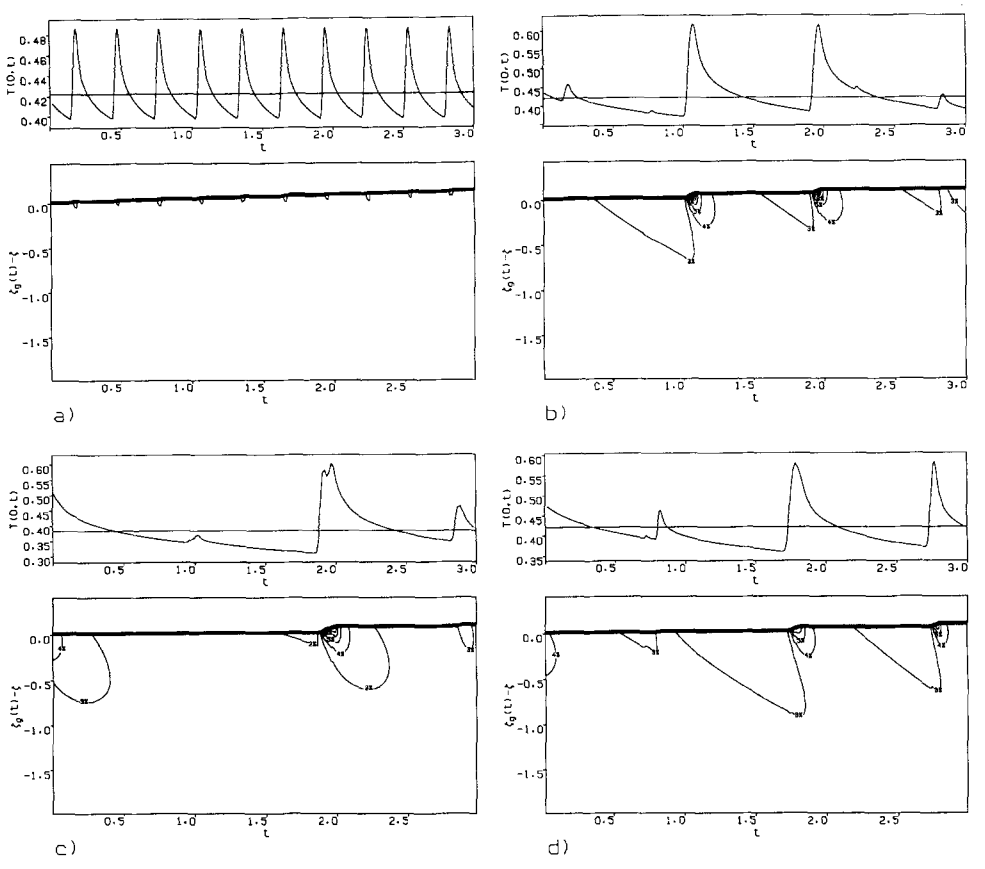

Fig. 6. Surface and far-field temperatures, billet growth and sub-surface isotherms: a) $r = 0$, b) $r = 0.25$, c) $r = 0.5$, d) $r = 0.75$. All figures $t_s = 5/17$.

time interval $\Delta t = 1$. Fig. 8 shows the same results for $\epsilon = 3.333 \times 10^{-4}$, computed over a time interval $\Delta t = 9$.

The first point to note is that the far field temperatures are the same at each radial position for each of the three different values of ϵ explored; solution of (43) is independent of ϵ. The change in different rotation and scanner rates has two effects on the boundary layer heat flow. Firstly, for smaller ϵ the surface temperature fluctuations become shorter and more frequent, with the amplitude of fluctuations about the far-field temperatures becoming smaller. Secondly, below the billet surface the depth of penetration of the thermal pulses is also significantly reduced with ϵ. This is particularly noticeable at the billet centre, Figs. 7a and 8a, where for small ϵ the boundary layer temperature becomes nearly constant. For the larger value of ϵ it is apparent that the effects from one thermal spray pulse can persist until the next pulse arrives. Additionally, the long pulse duration can allow considerable fluctuations in the surface temperature to occur, (e.g. Fig. 7d).

4.3. CHANGES IN CROWN SHAPE

The billet crown shape illustrated in Fig. 4b is special, in being nearly horizontal for nearly the entire billet radius. In practice the billet crown shape is usually more convex and changes shape, both during a process run and between process runs; concave billet crown shapes are

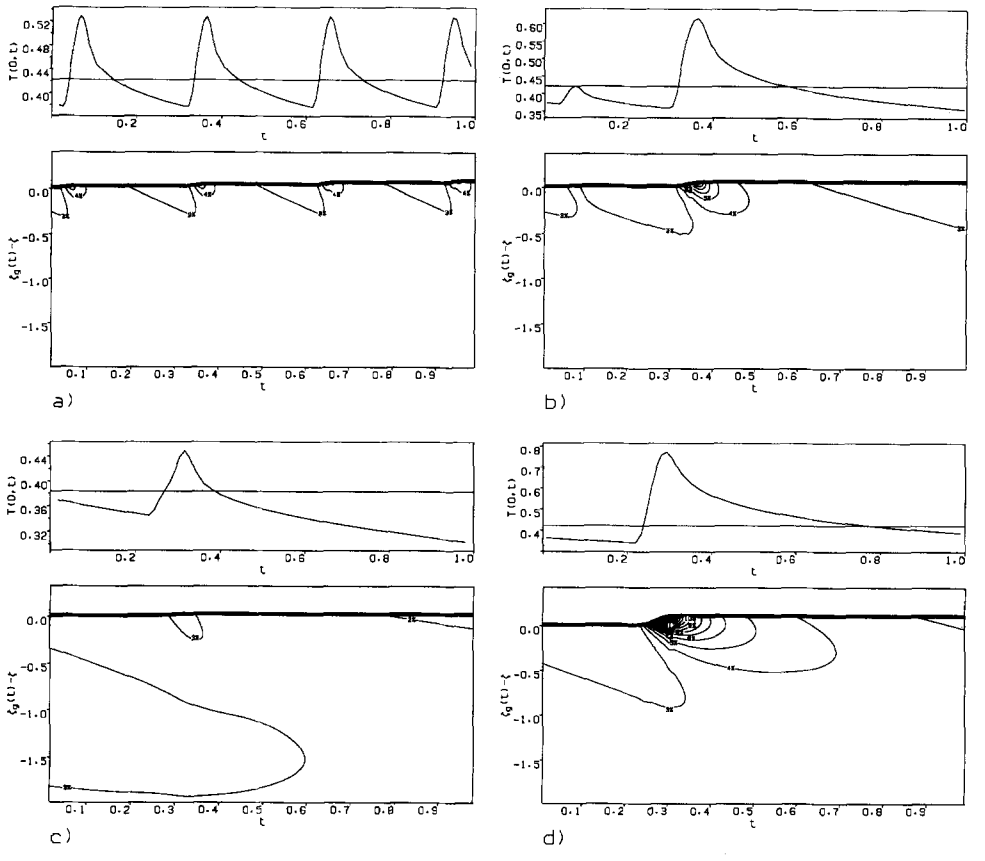

Fig. 7. Surface and far-field temperatures, billet growth and sub-surface isotherms: a) $r = 0$, b) $r = 0.25$, c) $r = 0.5$, d) $r = 0.75$. All figures: $\Delta t = 1$, $t_s = 5/17$, $\epsilon = 3 \times 10^{-3}$.

also possible. It is natural to ask how changing crown shapes affect the heat flow close to the billet surface. To examine these effects, similar computations to those in section 4.1 have been undertaken, but assuming now that the underlying billet shape is different.

The scanner function $\alpha(t)$ remains that of Fig. 4a and the atomiser is again scanned through the angles $\alpha_1 + \alpha_2\alpha(t)$, but now scanning ranges $\alpha_2 = 3°$ and $\alpha_2 = 9°$ are employed. The spray cone radius is kept at $r_s = 1/3$, also $t_s = 5/17$ and $\epsilon = 10^{-3}$. As before, constant mass flow rates and withdrawal rates, $\dot{m} = 1$ and $u = 1$, are assumed. After an $O_S(\epsilon^{-1})$ time interval the averaged billet growth grows towards the steady state shapes shown in Figs. 9a & b, and the boundary layer heat flow is then computed for a time interval $\Delta t = 3$.

It can be seen that the change in scanning range produces a considerable change in billet shape. For the 3° scanning range the steady crown is largely concave, whilst for the 9° scanning range it is convex. The boundary layer heat flow for the concave and convex steady states is shown in Figs. 10 and 11, respectively, again computed at the four radial distances $r = 0$, 0.25, 0.5 & 0.75.

First note that in both cases there is a considerable change in the surface normal vector as r increases. The "flower pattern" picture Fig. 4c, if drawn for both surfaces in Fig. 9 is quite similar. Thus, not surprisingly, Figs. 10a and 11a are almost identical, (see also Fig. 6a). Close to $r = 0$ the surface is horizontal and at $r = 0$ the averaged surface normal velocity is identically $(\epsilon Pe)^{1/2}$ in each case. Therefore the far-field temperatures are identical. Note

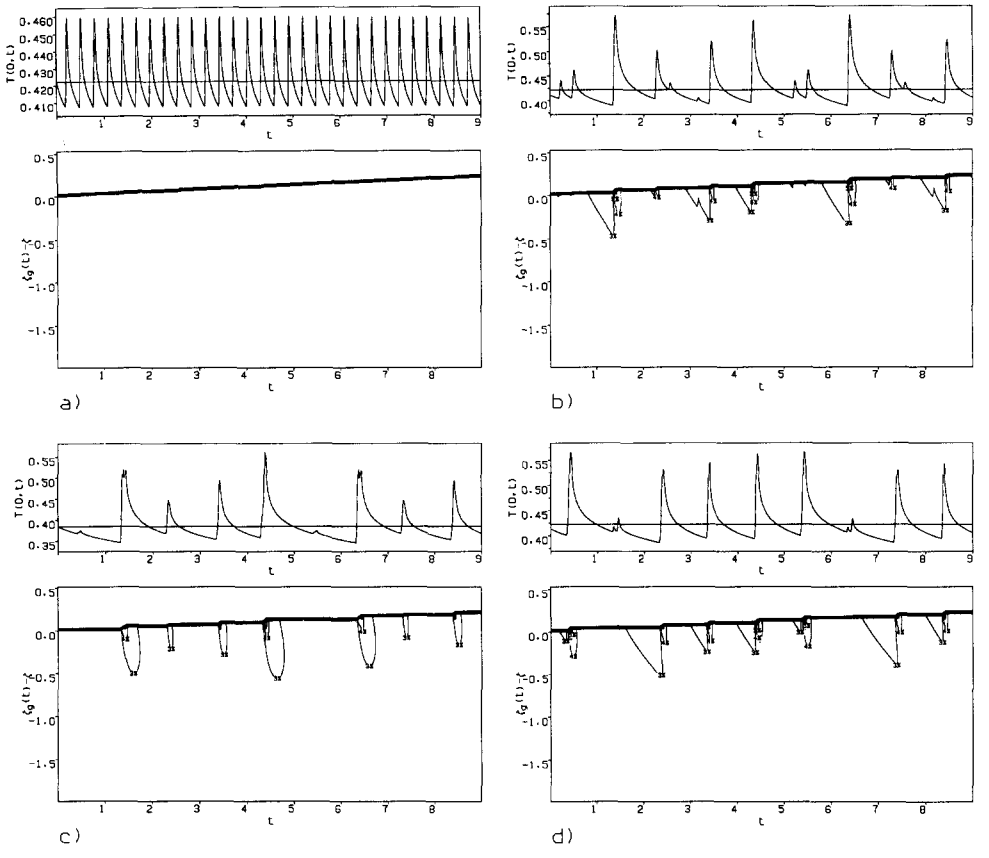

Fig. 8. Surface and far-field temperatures, billet growth and sub-surface isotherms: a) $r = 0$, b) $r = 0.25$, c) $r = 0.5$, d) $r = 0.75$. All figures: $\Delta t = 9$, $t_s = 5/17$, $\epsilon = 3.333 \times 10^{-4}$.

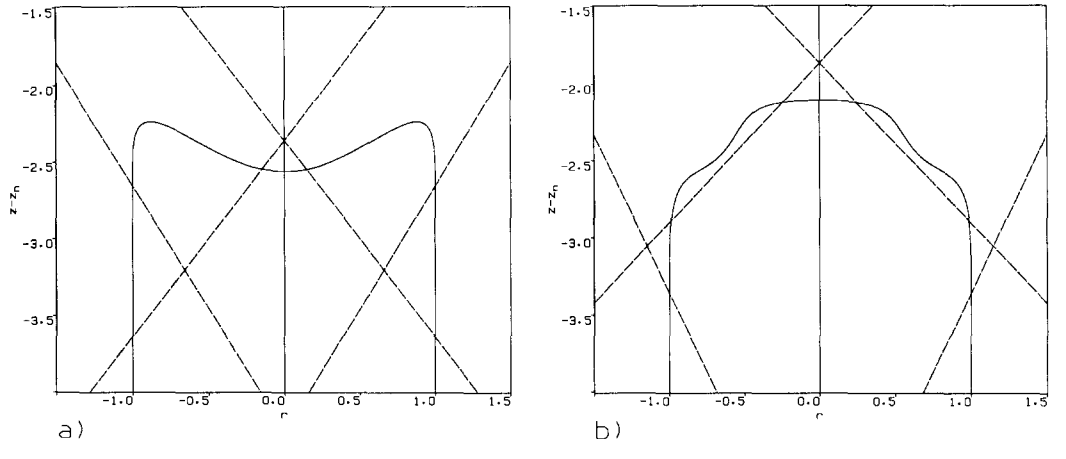

Fig. 9. Steady state billet crown shapes for fixed scanning angle $\alpha_1 = 35°$, spray cone radius $r_s = 1/3$, $g(r')$ a truncated normal distribution; a) scanning range, $\alpha_2 = 3°$, a) scanning range, $\alpha_2 = 9°$.

that if non-steady averaged growth were considered, one would be able to achieve different far-field temperatures.

Variations in boundary layer heat flow between Figs. 10b, c & d are not great. The slope of the billet surface is steeper at $r = 0.5$, and this is reflected in the lower far-field temperature.

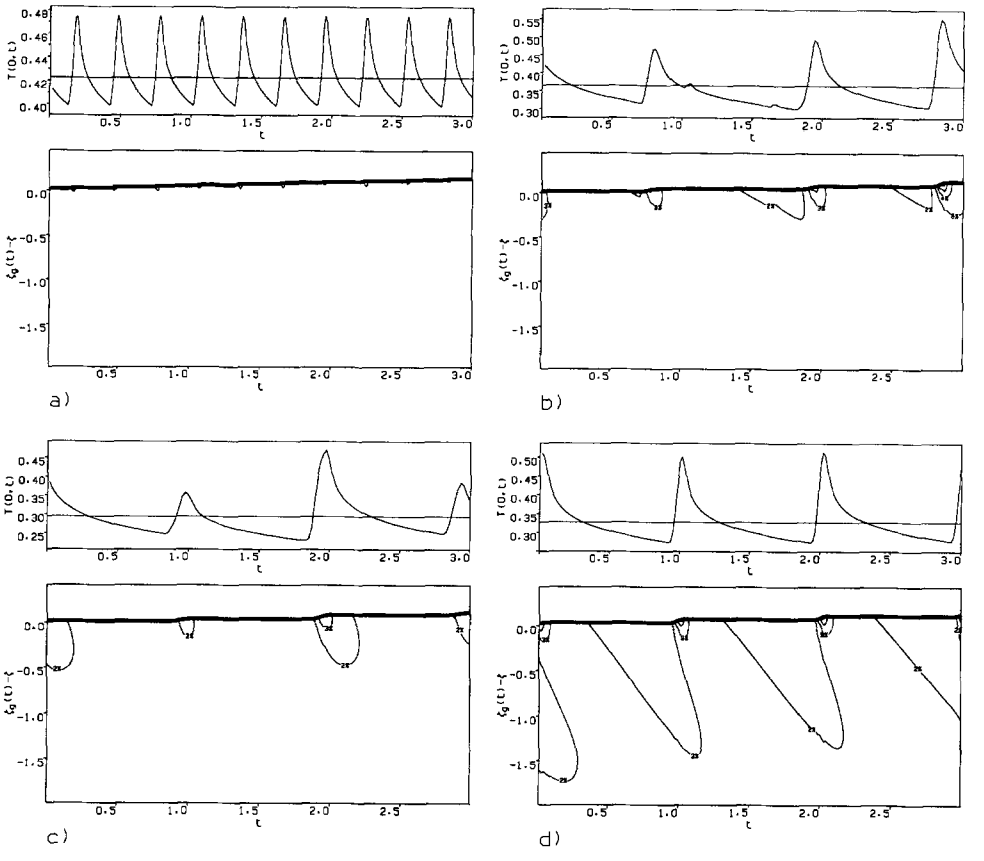

Fig. 10. Surface and far-field temperatures, billet growth and sub-surface isotherms: a) $r = 0$, b) $r = 0.25$, c) $r = 0.5$, d) $r = 0.75$. All figures: $\Delta t = 3, t_s = 5/17, \epsilon = 10^{-3}, \alpha_1 = 35°, \alpha_2 = 3°$.

The penetration depths of the heating spray pulses are approximately the same in each case, but at $r = 0.75$ the spray is delivered less frequently and this allows a very deep cooling pulse between depositions.

In sharp contrast to Figs. 10b, c & d, there are considerable differences in the boundary layer heat flow between Figs. 11b, c & d. At radial distances of $r = 0.25$ and $r = 0.75$ the billet crown is not particularly steep and the heat flow is quite similar to that shown in Figs. 10b & d. In Fig. 11c there is a massive fall in the far-field temperature, due solely to the steep slope of the billet crown. Between deposition periods the billet surface cools to about 25°C below the solidus temperature, and then rises 15 – 20°C above solidus during deposition. This seemingly massive temperature fluctuation is explained by the ratio $\hat{L}/\hat{c}\Delta\hat{T} \approx 3$; i.e. above the solidus temperature a given temperature fluctuation requires a corresponding internal energy fluctuation ≈ 4 times as large as it would below the solidus temperaure. Thus, the energy fluctuations at $r = 0.5$ are not so different to those found at $r = 0.25$ & 0.75, although the temperature fluctuation is considerable.

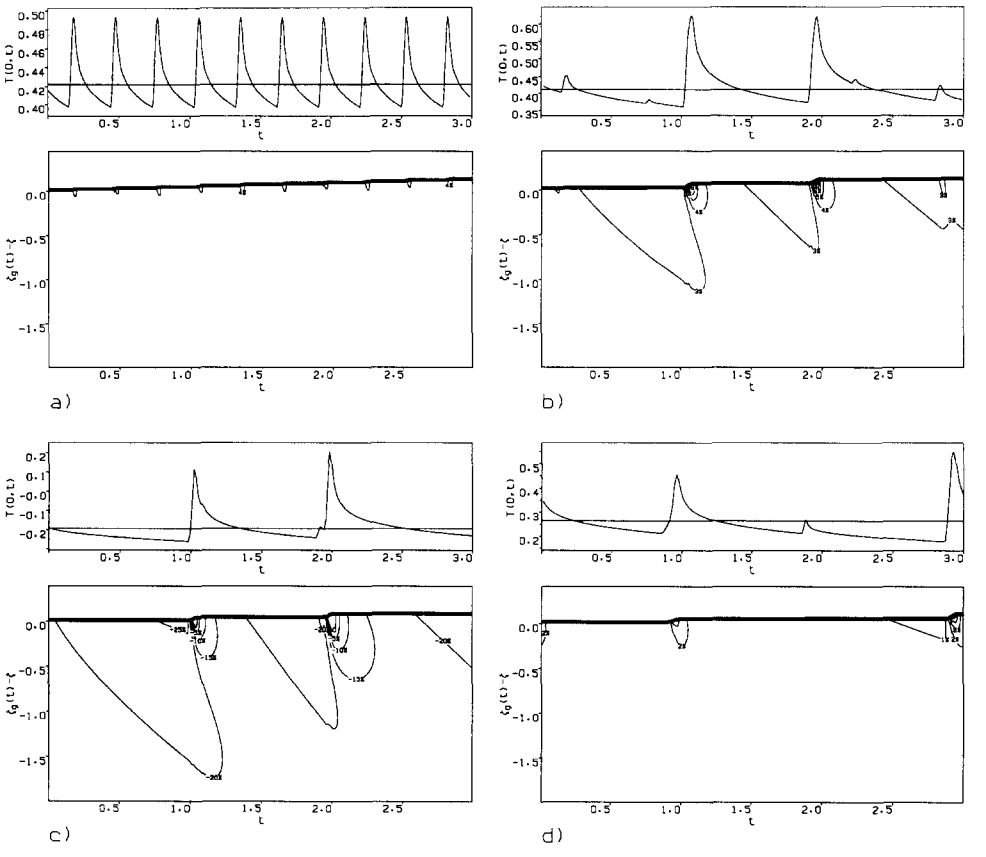

Fig. 11. Surface and far-field temperatures, billet growth and sub-surface isotherms: a) $r = 0$, b) $r = 0.25$, c) $r = 0.5$, d) $r = 0.75$. All figures: $\Delta t = 3$, $t_s = 5/17$, $\epsilon = 10^{-3}$, $\alpha_1 = 35°$, $\alpha_2 = 9°$.

4.4. CHANGING t_s

In all the previous results the ratio of scanner to rotation periods t_s has been kept constant. Although it is not sensible to change t_s on-line, it is of interest to examine whether one can change t_s so that $v(t)$ is altered at some radial positions and not at others.

In section 4.2 it was shown that by changing ϵ one could, in a fairly uniform way, affect the penetration depths and pulse durations across the full radius of the billet. It is assumed that a certain amount of reheating/remelting is good for the billet microstructure, since otherwise one must deposit exactly the right amount of spray in exactly the right condition at each point. At the billet centre $r = 0$ the frequent regular pulses do not penetrate very far below the surface, and this restricts the range of variation in ϵ which it is practical to make.

Ideally, one would therefore like to make the typical pulse pattern more similar, (i.e. in terms of length and duration), at different radial positions on the billet surface, so that one can vary ϵ and control the changes in heat flow uniformly across the billet surface. Really, one would like to do this in a way that is somehow optimal, but here "optimal" is rather hard to define. Instead it is shown what sort of effects can be achieved very simply. Fig. 12 shows the "flower pattern" that results from a $t_s = 10/11$, with the same steady state as in Fig. 4b.

Following this simple change, it can be seen from Fig. 12 that the centre of the billet will be hit by the spray about once on every rotation, whilst most other points will be hit either

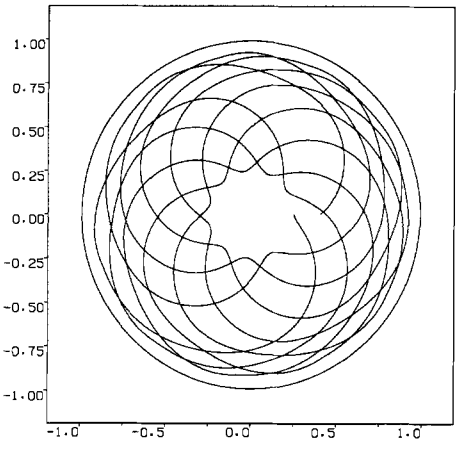

Fig. 12. Locus of the intercept of the spray cone axis with the steady state surface shown in Fig. 4b: $t_s = 10/11$; $\alpha_1 = 35°, \alpha_2 = 6°$.

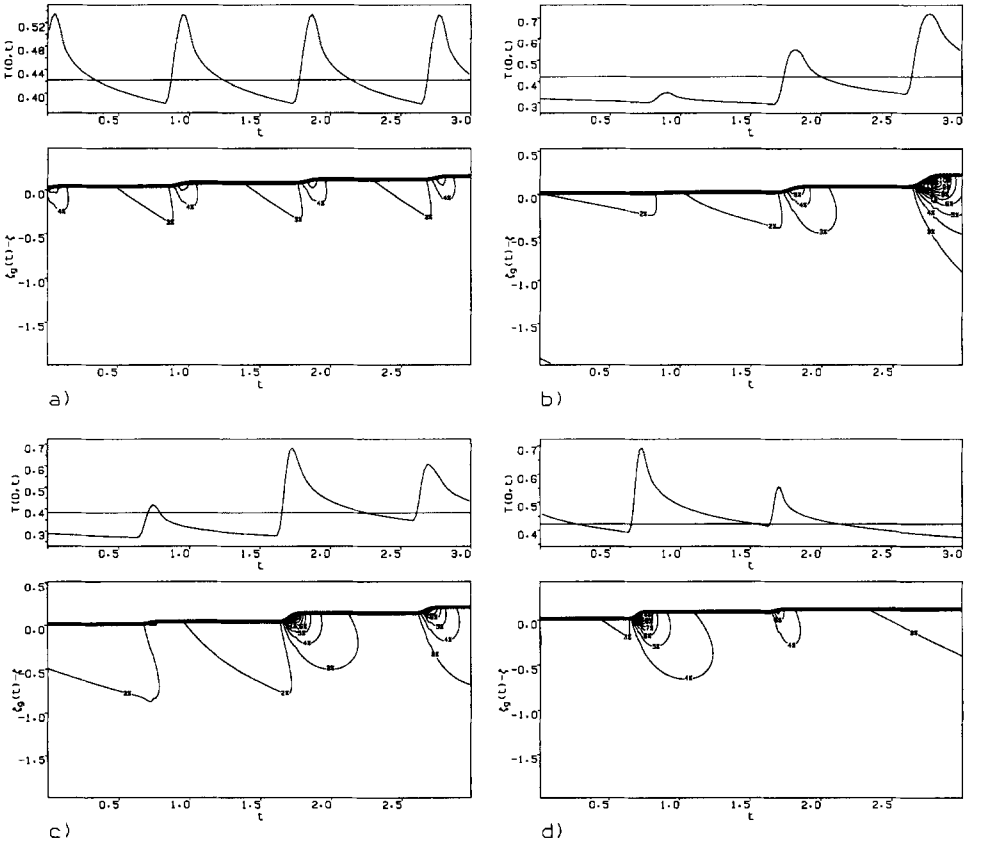

Fig. 13. Surface and far-field temperatures, billet growth and sub-surface isotherms: a) $r = 0$, b) $r = 0.25$, c) $r = 0.5$, d) $r = 0.75$. All figures: $\Delta t = 3, t_s = 10/11, \epsilon = 10^{-3}, \alpha_1 = 35°, \alpha_2 = 6°$.

zero or one times per rotation. The difference on the boundary layer heat flow is shown in Fig. 13; similar penetration depths and pulse durations now result at each radial distance.

5. Discussion

The main thrust of this paper has been to use a thermal boundary layer analysis to investigate questions of practical interest for an industrial metal forming process. The mathematical interest of the paper is two-fold. First, the model combines an asymptotic approximation to the fast timescale movement of the billet surface, (which is essentially an averaging method), with an asymptotic approximation to the heat flow near to the billet surface, (a boundary layer approximation). It is only for $Pe = O_S(1)$, (and of course $\epsilon \ll 1$), that the process timescales and length-scales invite this form of coupled approximation. Empirical evidence and heuristic argument for why $Pe = O_S(1)$ have been given.

The second point of mathematical interest is that the boundary layer approximation has been made with the boundary layer thickness measured in the direction normal to a boundary which is itself slowly moving. This slow movement means that the material coordinates of points within the boundary layer change after a significantly long time, and so the boundary layer approximation is expected to be only valid for short time intervals. This feature has not been seen by the author before, (although it seems likely that it is shared by other problems). Matching of the boundary layer approximation with an outer expansion has not been undertaken, since the boundary layer approximation has proven to be a very useful tool on its own.

The computational economy of the boundary layer approximation can not be understressed; this is the main motivation for the method. Using the boundary layer approximation requires the following steps. (i) The solution of the slow-time billet growth equations: a first order partial differential equation integrated over an $O(1)$ slow-time interval. (ii) The solution of one nonlinear equation to find a suitable azimuthal angle for boundary layer computation. (iii) The solution of another nonlinear equation to set the initial conditions. (iv) Finally, the integration of a one-dimensional nonlinear parabolic partial differential equation, over an $O(1)$ fast-time interval. To answer similar questions regarding sub-surface heat flow, without utilising boundary layer and averaging approximations, requires the integration of a three-dimensional nonlinear parabolic equation within an expanding domain, over an $O(\epsilon^{-1})$ fast-time interval.

5.1. Physical relevance

Before discussing the computed results, the utility of the boundary layer approximation is considered in a slightly wider sense. Considered dimensionally, the boundary layer length-scale is $\sim R(\epsilon/Pe)^{1/2}$ which for a 0.15m radius billet is of the order of 3-4 millimetres. Semi-solid spray droplets with mean diameter $\sim 80\mu$m which hit the surface can be estimated to "splat" to thicknesses in the approximate range[6]

$$5 - 10\ \mu\text{m},$$

(see discussion in [22]). Thus, the scale of isotherm penetration that has been seen in the numerical results, suggests that remelting and refreezing processes occur across

$$\sim 10^2,$$

flattened layers of deposited droplets. This implies some validity in (implicitly) using the continuum hypothesis over the boundary layer length-scale. One could argue that in certain cases such an hypothesis breaks down at the splat length-scale. This might be true, for example,

when deposition conditions are "too dry" and significant intersticial porosity develops. In this case one perhaps needs to consider modifying the thermal conductivity to account for inter-splat thermal contact resistance and/or abandoning the continuum hypothesis altogether and computing on the splat scale. Fortunately, in billet spray-forming such microstructures are usually only found close to the collector, where there is extremely rapid cooling of the spray initially deposited.

A second comment here is to note that the dimensional cooling rates of the surface following spray deposition are $\sim 10^2 - 10^3$°C/s; i.e. just bordering on the cooling regimes which are found in other rapid solidification processes. Droplet cooling rates of $\sim 10^3$°C/s and larger are known to exist in the spray, [32, 33], whereas cooling rates ~ 1°C/s can be estimated for the bulk billet. Therefore, this suggests that the (near) rapid solidification regime extends into the boundary layer, and it is only deeper below the billet surface that the much slower cooling takes over. Previous modelling of spray-forming processes has not really exposed this feature, since it has generally considered continuous deposition from the spray and/or thin deposits have been modelled.

Lastly, the analogy between the model used here and models of other processes such as pulsed laser heating is mentioned, see e.g. [34, 35, 36, 37]. Although there are similarities, there are also considerable differences. In particular, the power density levels found in pulsed laser heating applications are usually higher than in spray-forming and in spray-forming the energy pulse is also a mass pulse. This means that convection is an inherent part of the thermal problem in spray-forming.

5.2. COMPUTED RESULTS

The first thing that the numerical results clearly illustrate is that the local pattern of deposition experienced is extremely complex. One is often tempted to look at simplified cases, (e.g. suppose that the deposition is a regular pulse which hits each spot once per rotation). Such simplifications made here clearly avoid the true nature of the problem.

Different points typically receive an irregular pattern of interspersed large and small pulses, except at the centre where regularity is preserved. This complexity can cause problems for conventional (qualitative) understanding of the relationship between local deposition conditions and subsequent microstructure. Commonly, four different combinations of droplet and deposit thermal conditions are distinguished, each of which is related to a characteristic microstructure, see [15, 18]. Changes from one microstructural regime to the next result as both the spray and billet become hotter. This qualitative understanding has arisen largely from investigating one-dimensional and/or continuously growing thin deposits, where one is able to talk sensibly of a uniform "layer thickness" or "growth rate", at all points on the deposit. In billet spray-forming, the numerical results have shown that this characterisation is not directly applicable. Intermittency and irregularity of the spray pulse mean that a single surface location might experience a number of different microstructural regimes in quick succession. Correspondingly, porosity levels within spray-formed billets are found to exhibit complex local variations which are hard to characterise, [21]. The model approximation used here, at the very least, represents a useful tool for trying to understand some of these variations, both qualitatively and quantitatively.

5.2.1. *Process variations*

The results of sections 4.1 and 4.2 are supported by microstructural analysis and experimental investigations by Mingard, on billets sprayed under quite similar process conditions, [21]. Radial variations in porosity have been found at radial distances at which there are correspondingly sharp changes in surface gradient. Additionally, variation of rotation rate, (through a similar range to that in section 4.2), was found to produce high levels of porosity in the deposited material for both unusually high and low rotation rates. The porosity found at the high rotation rates seemed to result from a "dry" microstructure, with little bonding between layers. At very low rotation rates there was evidence of the porosity being caused by fluid instability on the billet surface, with gas pores found in the sprayed deposit on analysis.

There are two interesting feature of the results in section 4.3. First of all, the implication of the large difference between Figs. 11b, c & d, is that if the far-field boundary layer temperature is significantly below the solidus temperature, (i.e. "cold"), then one should find much noisier surface temperature measurements at a surface point than one should find at a point where the far-field boundary layer temperature is above the solidus temperature, (i.e. "hot"). The second point to be made clear is that the main difference between the boundary layer heat flow results in the two billets shown has nothing to do with convexity/concavity of the billet crown. For any non-horizontal billet crown, there are clearly going to be differences in the far-field boundary layer temperature resulting from changes in the slope of the billet crown. There will also be significant changes in the spray enthalpy with flight distance from the atomiser, (in this sense the concave billet crown is perhaps worse than the convex billet crown). All these variations are in a sense unavoidable. What the results here do show is that large local changes in the curvature of the billet crown are bad, (i.e. as in Fig. 11c).

In section 4.4 some simple attempts at improving the uniformity of spray deposition patterns across the billet surface were made. What was not explored was the effect that the changes made in section 4.4 might have had on the asymmetry of spray deposition, i.e. variation of $v(t)$ with choice of ϕ_0. This represents an area with much potential for systematic future development. There are also many other areas open for investigation. Variations in h_{gas}, $\hat{T}_{gas}$ and $\hat{H}_{spray}$ have not been explored in this paper, and non-steady averaged growth is also interesting to consider.

A last comment is that since the essential feature of the boundary layer heat flow is that it oscillates about it's far-field value, it is of practical value to be able to solve (43) for all dimensional parameter values, to give a (computerized) "rule-of-thumb" as to what the effects are of changing h_{gas}, $\hat{T}_{gas}$ and $\hat{H}_{spray}$ at different points on a billet surface. This is not a difficult computational task.

Acknowledgements

This work was supported through a Teaching Company Associateship by Alcan International Ltd, Banbury, U.K. and the Oxford Centre for Advanced Materials and Composites, University of Oxford, (Grant Reference Number GR/F/12006). This financial support and permission from Alcan international to publish this article is gratefully acknowledged. The author would like to express his thanks to Drs. Peter Alexander, Brian Cantor and Oliver Jacobs for their supervision during the course of this research and to Dr. Ken Mingard for explaining many metallurgical terms in plain English.

The author also acknowledges support during the writing of this paper from the Austrian government; Fonds zur Förderung der Wissenschaftlichen Forschung, project number P09647-PHY.

Notes

[1] Deposition/spreading times for individual droplets $\approx 10^{-6} - 10^{-5}$s, [28, 29]. Thermal equillibriation between droplet and billet occurs over a timescale $\sim 10^{-4}$s, see in [22]. Both of these are much shorter than other process timescales.

[2] Radiation can be estimated to account for less than 10% of the total heat losses.

[3] Data supplied empirically, [30], functions then computed by the methods described in [22].

[4] The production rig produces several different alloys, and these are produced in batches to reduce the risk of cross-contamination of alloying elements. Batches of the same alloy may be separated by a period of months, during which time modifications in the process and/or in operating procedures may conceivably occur. This is illustrated well in Fig. 3 where the "operational" Peclet number shifts from about 1.8 to about 1.4, between earlier and later batches.

[5] Tangential thermal gradient should only result from either thermal gradients deep within the billet, or from spatial gradients in any of B_{gas}, T_{gas}, v_{x_P} or H_{spray}. Each of these should only vary significantly over the length-scale of the spray cone radius, $r_s = O_S(1)$.

[6] Note that although there is typically a wide droplet size range in the spray, the larger droplets are more liquid and have more inertia on impact, than the smaller ones. Thus, the "splatted" droplet thickness range is much smaller than the droplet diameter range in the spray.

References

1. R.H. Bricknell, The structure and properties of a nickel-base superalloy produced by Osprey atomisation-deposition, *Met. Trans.* 17A (1986) 583-591.
2. W. Kahl and J. Leupp, High performance aluminium produced by spray deposition, in proceedings of *International Conference on Spray Forming*, (1990) Swansea, U.K.
3. K.A. Kojima, R.E. Lewis and M.J. Kaufman, Microstructural characterization and mechanical properties of a spray-cast Al-Li-Cu-Mg-Zr alloy, in proceedings of *Aluminium Lithium 5 Conference*, (1992)
4. E.J. Lavernia and N.J. Grant, Structures and Properties of a Modified 7075 Aluminium Alloy Produced by Liquid Dynamic Compaction, *International Journal of Rapid Solidification*, 2 (1986) 93-106.
5. E.J. Lavernia, E. Gomez and N.J. Grant, The Structures and Properties of Mg-Al-Zr and Mg-Zn-Zr Alloy Produced by Liquid Dynamic Compaction, *Materials Science and Engineering*, 95 (1987) 225-236.
6. P.J. Meschter, J.K. Gregory, R.J. Lederich, J.E. O'Neal, E.J. Lavernia and N.J. Grant, Microstructures and properties of rapid solidification processed aluminium-high lithium alloys, *Journal de Physique*, 48-C3 (1987) 317-325.
7. K. Ogata, E.J. Lavernia, G. Rai and N.J. Grant, Structures and Properties of a Rapidly Solidified Superalloy Produced by Liquid Dynamic Compaction, *International Journal of Rapid Solidification*, 2 (1986) 21-35.
8. T.C. Willis, Spray deposition process for metal matrix composites manufacture, *Powder Metallurgy*, 31 (1988) 485-488.
9. A.J. Owen, Ultralite UL40 - The World's lowest density commercially available aluminium alloy, *Aluminium Industry*, 12 (1993) 24-25.
10. S. Annavarapu, Spray casting of steel strip: Modelling and experimental studies, *Ph.D. thesis*, Drexel University, (1989).
11. S. Annavarapu, D. Apelian and A. Lawley Spray casting of steel strip: Process analysis, *Met. Trans.*, 21A (1990) 3237-3255.
12. P.S. Grant, Spray forming of aluminium alloys, *D.Phil. thesis*, Oxford University, (1991).
13. E.M. Gutierrez, E.J. Lavernia, G.M. Trapaga and J. Szekely, A mathematical model of the Liquid Dynamic Compaction process. Part 2: Formation of the deposit, *International Journal of Rapid Solidification*, 4 (1988) 125-150.
14. E.M. Gutierrez, E.J. Lavernia, G.M. Trapaga, J. Szekely and N.J. Grant, A mathematical model of the spray deposition process, *Met. Trans.*, 20A (1989) 71-85.
15. P. Mathur, Analysis of the spray deposition process, *Ph.D. thesis*, Drexel University, (1988).
16. P. Mathur, S. Annavarapu, D. Apelian and A. Lawley, Process control, modelling and applications of spray casting, *Journal of Metals*, 41 (1989) 23-28.

17. P. Mathur, D. Apelian and A. Lawley, Analysis of the spray deposition process, *Acta Metall.*, 37 (1989), 429-443.
18. E.J. Lavernia, The evolution of microstructure during spray atomisation and deposition, *International Journal of Rapid Solidification*, 5 (1989), 47-85.
19. A.R.E. Singer and R.W. Evans, Incremental solidification and forming, *Metals Technology*, 10 (1983), 61-68.
20. P.W. Alexander, confidential report to Alcan-Oxford TCS grant GR/F/12006, February (1991).
21. K.P. Mingard, Alcan-Oxford TCS grant GR/F/12006, Metallurgical quality control reports, October (1990) - October (1992).
22. I.A. Frigaard, Mathematical modelling of an aluminium spray process, *D.Phil. thesis*, Oxford University, (1993).
23. I.A. Frigaard, The Dynamics of Spray-formed Billets, *SIAM J. Appl. Math.* 55(5) (1995) 1161–1203.
24. I.A. Frigaard, Growth Dynamics of Spray-formed Aluminium Billets, Part 1; Steady State Crown Shapes, *Journal of Materials Processing and Manufacturing Science*, 3 (1994), 173-193.
25. I.A. Frigaard, Growth Dynamics of Spray-formed Aluminium Billets, Part 2; Transient Billet Growth, *Journal of Materials Processing and Manufacturing Science*, 3 (1995) 257–275.
26. I.A. Frigaard and O. Scherzer, Growing the Perfect Billet, *SIAM J. Appl. Math.*, accepted for publication.
27. P. Mathur, S. Annavarapu, D. Apelian and A. Lawley, Spray casting: an integral model for process understanding and control, *Materials Science and Engineering*, A142 (1991) 261-276.
28. J. Madejski, Solidification of droplets on a cold surface. *International Journal of Heat and Mass Transfer*, 19 (1976) 1009-1013.
29. G.M. Trapaga and J. Szekely. Mathematical Modeling of the Isothermal Impingement of Liquid Droplets in Spraying Processes, *Metall. Trans.*, 22B (1991) 901-914.
30. P.S. Grant and B. Cantor, Contract work for Alcan International Ltd., Banbury, U.K.; communication of 29th May, (1990).
31. P.C. Meek and J. Norbury, Two-stage, two-level finite difference schemes for non-linear parabolic equations. *I.M.A. Journal on Numerical Analysis*, 2 (1982) 335-356.
32. S. Rogers and L. Katgerman, Heat transfer and solidification of a stream of molten metal during atomisation by an impinging gas jet, Proceedings of the *5th International conference on numerical methods in thermal problems*, Montreal, (1987), 1806-1817.
33. P.S. Grant, B. Cantor, S. Rogers and L. Katgerman, A computer model for droplet and particle trajectories and thermal profiles in spray forming, *Cast Metals*, 3 (1991) 227-232.
34. D.J. Sanders, Temperature beams produced by scanning Gaussian laser beams, *Applied Optics*, 23(1) (1984) 30-35.
35. M.N. Yakunkin, Investigation of temperature fluctuations due to periodic heating by a laser pulse, Translated from *Teplofizika Vysokikh Temperatur*, 26(4) (1988) 759-766.
36. P. Ravi Vishnu, W.B. Li and K.E. Easterling, Heat flow model for pulsed welding, *Materials Science and Technology*, 7 (1991) 649-659.
37. I.Y. Smurov, A.A. Uglov, A.M. Lashyn, P. Matteazzi, L. Covelli and V. Tagliaferri, Modelling of pulse-periodic energy flow action on metallic materials, *Int. J. Heat Mass Transfer*, 34 (1991) 961-971.